

# Universality classes of the Anderson transition in three-dimensional symmetry classes AIII, BDI, C, D and CI

Tong Wang,<sup>1,2</sup> Tomi Ohtsuki,<sup>3</sup> and Ryuichi Shindou<sup>1,2,\*</sup>

<sup>1</sup>*International Center for Quantum Materials, School of Physics, Peking University, Beijing 100871, China*

<sup>2</sup>*Collaborative Innovation Center of Quantum Matter, Beijing 100871, China*

<sup>3</sup>*Physics Division, Sophia University, Chiyoda-ku, Tokyo 102-8554, Japan*

(Dated: May 7, 2021)

We clarify universal critical properties of delocalization-localization transitions in three-dimensional (3D) unitary and orthogonal classes with particle-hole and/or chiral symmetries (classes AIII, BDI, D, C and CI). We first introduce tight-binding models on cubic lattice that belong to these five nonstandard symmetry classes respectively. Unlike the Bogoliubov-de Gennes Hamiltonian for superconductors, all the five models have finite areas of Fermi surfaces in the momentum space in the clean limit. Thereby, the scaling theory of the Anderson transition guarantees the presence of the delocalization-localization transitions at finite disorder strength in these models. Based on this expectation, we carry out extensive transfer matrix calculations of the Lyapunov exponents for zero-energy eigenstates of the disordered tight-binding models with quasi-one-dimensional geometry. Near the Anderson transition point, the correlation length diverges with a universal critical exponent  $\nu$ . Using finite-size scaling analysis of the localization length, we determine the critical exponent of the transitions and scaling function of the (normalized) localization length in the three non-standard unitary symmetry classes:  $\nu_{\text{AIII}} = 1.06 \pm 0.02$ ,  $\nu_{\text{D}} = 0.87 \pm 0.03$ , and  $\nu_{\text{C}} = 0.996 \pm 0.012$ . Our result of the class C is consistent with a previous study of classical network model [M. Ortuño et al, Phys. Rev. Lett. **102**, 070603 (2009)]. The critical exponents of the two non-standard orthogonal classes are estimated as  $\nu_{\text{CI}} = 1.17 \pm 0.02$  and  $\nu_{\text{BDI}} = 1.12 \pm 0.06$ . Our result of the class CI is consistent with another previous study of a lattice model, while the exponent of the class BDI is at variance with the previous evaluation of nodal Dirac ring model [X. L. Luo et al, Phys. Rev. B. **101**, 020202(R) (2020)].

## I. INTRODUCTION

The quantum interference of two counter-propagating waves form a standing wave that does not move in space, suppressing particle diffusions completely in random media. After Anderson's seminal proposal of the localization of electron wavefunctions in disordered solids [1–3], theoretical understandings of the localization phenomena have been elaborated by scaling theories [4, 5], field theories [6–10], numerical simulations [11–14], and symmetry classifications of random matrices [15–18]. It is widely acknowledged that delocalization-localization (Anderson) transition occurs in a variety of physical systems, including many-body electronic systems [19–21], Bose–Einstein condensates [22–24], and classical optical [25–30] and acoustic systems [31–33]. The Anderson transition is a continuous quantum phase transition. Like other second-order phase transitions in statistical physics, the quantum phase transitions are categorized by universality classes. Each universality class is characterized by universal critical exponent and scaling functions, the information of which is encoded into scaling properties of an effective field theory around its fixed points. It is widely believed that the universality class of the Anderson transition is determined only by symmetries of disordered Hamiltonian (random matrix) and spatial dimension of the system [4, 5].

The classification of Hermitian random matrices leads to ten symmetry classes known as the Altland-Zirnbauer (AZ) classes. They consist of standard Wigner-Dyson symmetry classes (A, AI, AII), three chiral symmetry classes (AIII, BDI, CII) [9, 10], and four Bogoliubov-de Gennes (BdG) symmetry classes (D, C, DIII, CI) [18, 38]. The random matrices and disordered Hamiltonian in the non-standard symmetry classes not only describe universal aspects of the localization of Bogoliubov quasiparti-

	class	TRS	PHS	CS	$\nu$	Ref.
Unitary	A	No	No	No	$1.443 \pm 0.003$	[34]
Orthogonal	AI	1	No	No	$1.572 \pm 0.003$	[35]
Symplectic	AII	-1	No	No	$1.37 \pm 0.01$	[36]
Chiral Unitary	AIII	No	No	Yes	$1.06 \pm 0.02$	*
Chiral Orthogonal	BDI	1	1	Yes	$1.12 \pm 0.06$	*
Chiral Symplectic	CII	-1	-1	Yes	–	–
BdG	D	No	1	No	$0.87 \pm 0.03$	*
	C	No	-1	No	$0.996 \pm 0.012$	*
	DIII	-1	1	Yes	$1.1 \pm 0.05$	[37]
	CI	1	-1	Yes	$1.17 \pm 0.02$	*

TABLE I. Classification according to time reversal symmetry (TRS), particle-hole symmetry (PHS), chiral symmetry (CS), and their universal critical exponents  $\nu$  in 3D Anderson transition. TRS is defined as  $\mathbb{T}\mathbb{H}^T\mathbb{T}^{-1} = \mathbb{H}$  and PHS as  $\mathbb{C}\mathbb{H}^T\mathbb{C}^{-1} = -\mathbb{H}$ . For TRS (PHS) 1 mean  $\mathbb{T}^T = \mathbb{T}$  ( $\mathbb{C}^T = \mathbb{C}$ ) whereas -1 means  $\mathbb{T}^T = -\mathbb{T}$  ( $\mathbb{C}^T = -\mathbb{C}$ ). \* indicates the values estimated in this paper, whereas – indicates yet to be determined.

\* rshindou@pku.edu.cn

cle wavefunctions in disordered superconductors [18, 38] but also they are closely related to the localization of classical waves in random dissipative media [39], non-Hermitian disordered systems, which are attracting a lot of research interests during the last couple of years [40–47]. As some will be demonstrated for the first time in this paper, three-dimensional (3D) models in each symmetry class show the delocalization-localization transition and its quantum criticality is characterized by its own universal scaling functions and the critical exponent. So far, the critical exponent of the 3D Anderson transition in seven out of the ten AZ classes have been studied numerically. They are the three Wigner-Dyson classes A, AI and AII [34–36]; the chiral orthogonal class BDI [48]; and three BdG classes C [49], CI [48], and DIII [37], while the other three (AIII, CII, D) remain to be clarified. Numerical values of the critical exponent of these classes, including those evaluated in this paper, are listed in TABLE I.

In this article, we clarify the universal critical exponents and scaling functions associated with the localization length in the 3D Anderson transition of the symmetry classes AIII, BDI, C, D and CI, using transfer matrix method. The chiral class AIII has topological phases classified by integer winding number in  $d = 1, 3$  dimension(s). The study of the class AIII was rather established both numerically and analytically in 1D [50–54], but most of them focused on topological quantum critical point and few were directed to localization phenomena in 3D class AIII systems. Class C and D in 3D are also less studied than in 2D, where there exists 2D spin and thermal quantum Hall insulator phases in these two symmetry classes, respectively. Low-energy Bogoliubov excitations in spin-triplet superconductors with broken time-reversal symmetry  $\text{Sr}_2\text{RuO}_4$  [55, 56] and  $\text{UPt}_3$  [57] potentially belong to these two non-standard symmetry classes in 3D.

In this paper, we propose two-band tight-binding models on the cubic lattice that belong to symmetry classes AIII, BDI, C, D and CI respectively, which enable precise simulation studies of the 3D Anderson transition. Critical exponents of the Anderson transition in the 3D classes AIII and D are estimated for the first time, whose values are distinct from those of the other known symmetry classes. Our estimates of exponents for the classes C and CI agree with previous works of a classical network model [49] and a lattice model [48].

## II. UNITARY MODELS WITH PARTICLE-HOLE OR CHIRAL SYMMETRIES

Let us first introduce the following two-orbital tight-binding model on the cubic lattice that is shared by all

the three unitary models studied in this paper:

$$\begin{aligned}
 H_0 &\equiv \sum_{\mathbf{i}, \mathbf{j}} \sum_{d, d'=a, b} |\mathbf{i}, d\rangle [\mathbb{H}_0]_{(\mathbf{i}, d | \mathbf{j}, d')} \langle \mathbf{j}, d| \\
 &= \sum_{\mathbf{i}} (\epsilon_{\mathbf{i}} + \Delta) (|\mathbf{i}, a\rangle \langle \mathbf{i}, a| - |\mathbf{i}, b\rangle \langle \mathbf{i}, b|) + \\
 &\sum_{\mathbf{i}} \left\{ t_{\perp} \left[ i (|\mathbf{i} + \mathbf{e}_x, a\rangle \langle \mathbf{i}, b| + |\mathbf{i} + \mathbf{e}_x, b\rangle \langle \mathbf{i}, a|) \right. \right. \\
 &\quad \left. \left. + (|\mathbf{i} + \mathbf{e}_y, a\rangle \langle \mathbf{i}, b| - |\mathbf{i} + \mathbf{e}_y, b\rangle \langle \mathbf{i}, a|) \right] \right. \\
 &\quad \left. + t_{\parallel} (|\mathbf{i} + \mathbf{e}_z, a\rangle \langle \mathbf{i}, a| + |\mathbf{i} + \mathbf{e}_z, b\rangle \langle \mathbf{i}, b|) + \text{H.c.} \right\}. \quad (1)
 \end{aligned}$$

Here  $\mathbf{i} \equiv (i_x, i_y, i_z)$  specifies the cubic-lattice site;  $\mathbf{e}_x \equiv (1, 0, 0)$ ,  $\mathbf{e}_y \equiv (0, 1, 0)$ , and  $\mathbf{e}_z \equiv (0, 0, 1)$ . The lattice constant is taken to be the unit length.  $a$  and  $b$  are the two orbitals:  $d, d' = a, b$ . The nearest neighbor (NN) hopping within the  $x$ - $y$  plane is an inter-orbital hopping  $t_{\perp}$ , and the NN hopping along  $z$  direction is an intra-orbital hopping  $t_{\parallel}$ .  $\pm\Delta$  is an onsite energy for the  $a, b$  orbitals respectively, and  $\epsilon_{\mathbf{i}}$  is a random potential independently distributed on each lattice site. In numerical simulations, we choose the distribution of the random potential to be uniform:  $\epsilon_{\mathbf{i}} \in [-W/2, W/2]$ ,  $\overline{\epsilon_{\mathbf{i}} \epsilon_{\mathbf{j}}} = \delta_{\mathbf{i}, \mathbf{j}} W^2/12$ . The tight binding Hamiltonian has the following chiral symmetries (Eqs. (2,3)) and particle-hole symmetries (Eqs. (4),(5)):

$$\mathbb{P}_1 \mathbb{H}_0 \mathbb{P}_1^{-1} = -\mathbb{H}_0, \quad \mathbb{P}_1 = \delta_{\mathbf{i}, \mathbf{j}} (-1)^{i_x + i_z} [\sigma_2]_{d, d'}, \quad (2)$$

$$\mathbb{P}_2 \mathbb{H}_0 \mathbb{P}_2^{-1} = -\mathbb{H}_0, \quad \mathbb{P}_2 = \delta_{\mathbf{i}, \mathbf{j}} (-1)^{i_y + i_z} [\sigma_1]_{d, d'}, \quad (3)$$

$$\mathbb{C}_1 \mathbb{H}_0^T \mathbb{C}_1^{-1} = -\mathbb{H}_0, \quad \mathbb{C}_1 = \delta_{\mathbf{i}, \mathbf{j}} (-1)^{i_z} [\sigma_1]_{d, d'}, \quad (4)$$

$$\mathbb{C}_2 \mathbb{H}_0^T \mathbb{C}_2^{-1} = -\mathbb{H}_0, \quad \mathbb{C}_2 = \delta_{\mathbf{i}, \mathbf{j}} (-1)^{i_x + i_y + i_z} [\sigma_2]_{d, d'}, \quad (5)$$

with  $\mathbb{P}_2 \equiv \mathbb{P}_1 \mathbb{C}_1 \mathbb{C}_2$ .  $\sigma_{1,2,3}$  are the Pauli matrices in the  $a, b$  orbital space and  $\sigma_0$  is the unit matrix. The combination of particle-hole symmetries and chiral symmetries gives the time-reversal symmetries, e.g.  $(\mathbb{P}_1 \mathbb{C}_1)^T \mathbb{H}_0^T \mathbb{P}_1 \mathbb{C}_1 = \mathbb{H}_0$ .  $\mathbb{P}_1 \mathbb{P}_2 \equiv \mathbb{C}_1 \mathbb{C}_2 = (-1)^{i_x + i_y} i \sigma_z$  commutes with  $\mathbb{H}_0$ , where the tight-binding Hamiltonian can be block-diagonalized in a basis of the real-valued eigenvectors of  $\mathbb{P}_1 \mathbb{P}_2$ . Since  $\mathbb{P}_1 \mathbb{C}_1$  and  $\mathbb{P}_1 \mathbb{C}_2$  commute with  $\mathbb{P}_1 \mathbb{P}_2$ ,  $\mathbb{P}_1 \mathbb{C}_1$  and  $\mathbb{P}_1 \mathbb{C}_2$  are block-diagonalized in the same basis, too. Accordingly, the two blocks of the tight-binding Hamiltonian are time-reversal symmetric. Since  $(\mathbb{P}_1 \mathbb{C}_1)^* (\mathbb{P}_1 \mathbb{C}_1) = +1$ ,  $H_0$  belongs to the orthogonal class. On the basis of such  $H_0$ , we will next introduce other parts of the hopping terms, which lead to the three unitary models belonging to the three non-standard symmetry classes one by one.

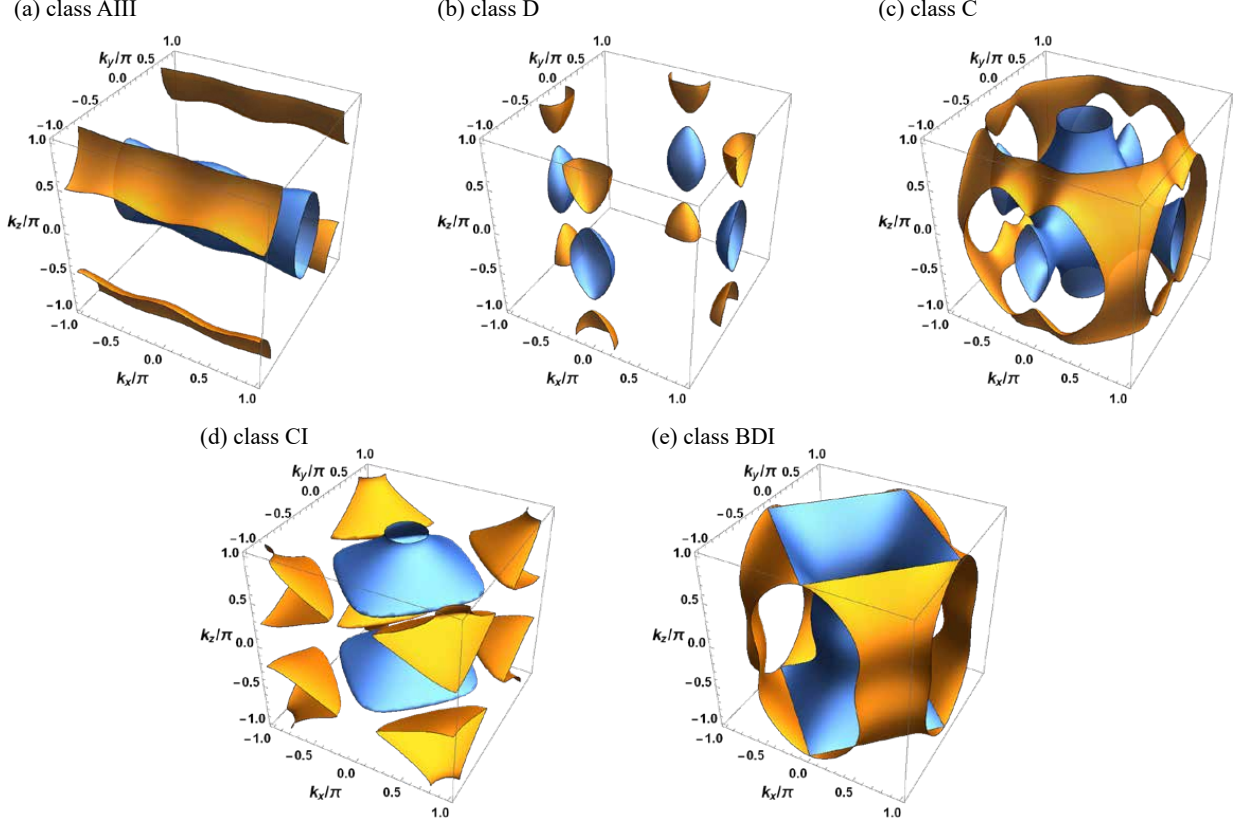


FIG. 1. Fermi surfaces of the two-bands models in the five non-standard symmetry classes at  $E = 0$  in the clean limit. The yellow surfaces are of the upper band, and the blue surfaces are of the lower band.

### A. Class AIII model

To break the two particle-hole symmetries, we add the following nearest neighbor hoppings within the  $x$ - $y$  plane;

$$\begin{aligned}
 H_{\text{AIII}} &\equiv \sum_{i,j} \sum_{d,d'=a,b} |\mathbf{i}, d\rangle [\mathbb{H}_{\text{AIII}}]_{(i,d|j,d')} \langle \mathbf{j}, d'| \\
 &= H_0 + \sum_i \left[ t_1 (|\mathbf{i} + \mathbf{e}_x, a\rangle \langle \mathbf{i}, a| - |\mathbf{i} + \mathbf{e}_x, b\rangle \langle \mathbf{i}, b|) \right. \\
 &\quad \left. + t_2 (|\mathbf{i} + \mathbf{e}_y, a\rangle \langle \mathbf{i}, a| + |\mathbf{i} + \mathbf{e}_y, b\rangle \langle \mathbf{i}, b|) + \text{H.c.} \right]. \quad (6)
 \end{aligned}$$

The model respects the chiral symmetry in Eq. (3), while the two particle-hole symmetries are broken by  $t_2$  and  $t_1$ , respectively. We set  $\Delta = 0.0$ ,  $t_\perp = 0.6$ ,  $t_\parallel = 0.4$ , and  $t_1 = t_2 = 0.5$ . The Hamiltonian in the clean limit is Fourier-transformed to

$$\begin{aligned}
 H_{\text{AIII}}(\mathbf{k}) &= 2(t_\parallel \cos k_z + t_2 \cos k_y) \sigma_0 + (\Delta + 2t_1 \cos k_x) \sigma_3 \\
 &\quad - 2t_\perp (\sin k_x \sigma_1 + \sin k_y \sigma_2), \quad (7)
 \end{aligned}$$

where the two bands are particle-hole symmetric under the translation of the momentum by  $(0, \pi, \pi)$ . The upper (lower) energy band forms an electron (hole) pocket at  $E = 0$  around the zone boundary (center) axis of  $(k_y, k_z) = (\pi, \pi)$   $((0, 0))$  (Fig. 1(a)).

### B. Class D model

To break the chiral symmetries and one of the two particle-hole symmetries (Eq. (5)), we add to  $H_0$  the following NN hoppings within the  $x$ - $y$  plane:

$$\begin{aligned}
 H_{\text{D}} &\equiv \sum_{i,j} \sum_{d,d'=a,b} |\mathbf{i}, d\rangle [\mathbb{H}_{\text{D}}]_{(i,d|j,d')} \langle \mathbf{j}, d'| \\
 &= H_0 + \sum_i \left[ t_1 (|\mathbf{i} + \mathbf{e}_x, a\rangle \langle \mathbf{i}, a| - |\mathbf{i} + \mathbf{e}_x, b\rangle \langle \mathbf{i}, b|) \right. \\
 &\quad \left. + t_2 (|\mathbf{i} + \mathbf{e}_y, a\rangle \langle \mathbf{i}, a| - |\mathbf{i} + \mathbf{e}_y, b\rangle \langle \mathbf{i}, b|) + \text{H.c.} \right]. \quad (8)
 \end{aligned}$$

The model respects the particle-hole symmetry in Eq. (4), while the two chiral symmetries are broken by  $t_1$  and  $t_2$ , respectively. We set  $\Delta = 0.1$ ,  $t_\perp = 0.3$ ,  $t_\parallel = 0.2$ , and  $t_1 = t_2 = 0.5$ . Since  $\mathbb{C}_1^T = \mathbb{C}_1$ , the model belongs to the symmetry class D. The tight-binding model can be regarded as layered Chern insulator models [58, 59]. In momentum space, the clean-limit Hamiltonian takes the following form

$$\begin{aligned}
 H_{\text{D}}(\mathbf{k}) &= 2t_\parallel \cos k_z \sigma_0 - 2t_\perp (\sin k_x \sigma_1 + \sin k_y \sigma_2) \\
 &\quad + (\Delta + 2t_1 \cos k_x + 2t_2 \cos k_y) \sigma_3. \quad (9)
 \end{aligned}$$

A finite  $t_\parallel$  closes the band gap at  $E = 0$ , where electron and hole pockets appears at  $k_z = 0$  and  $\pi$ , respectively,

as shown in Fig. 1(b).

### C. Class C model

To construct a class C model from Eq. (1), we add to  $H_0$  the following nearest neighbor hoppings within the  $x$ - $y$  plane:

$$\begin{aligned} H_C &\equiv \sum_{\mathbf{i}, \mathbf{j}} \sum_{d, d'=a, b} |\mathbf{i}, d\rangle [\mathbb{H}_C]_{(\mathbf{i}, d | \mathbf{j}, d')} \langle \mathbf{j}, d' | \\ &= H_0 + \sum_{\mathbf{i}} \left[ t_1 (|\mathbf{i} + \mathbf{e}_x, a\rangle \langle \mathbf{i}, a| + |\mathbf{i} + \mathbf{e}_x, b\rangle \langle \mathbf{i}, b|) \right. \\ &\quad \left. + t_2 (|\mathbf{i} + \mathbf{e}_y, a\rangle \langle \mathbf{i}, a| + |\mathbf{i} + \mathbf{e}_y, b\rangle \langle \mathbf{i}, b|) + \text{H.c.} \right]. \end{aligned} \quad (10)$$

The model respects the particle-hole symmetry Eq. (5) with  $\mathbb{C}_2^T = -\mathbb{C}_2$ , while finite  $t_1$  and  $t_2$  break Eq. (3) and (2), respectively. Therefore the model belongs to symmetry class C. In this paper we set  $\Delta = 0.1$ ,  $t_\perp = 0.6$ ,  $t_\parallel = 0.4$ , and  $t_1 = t_2 = 0.5$ . In the clean limit, this Hamiltonian is Fourier-transformed to

$$\begin{aligned} H_C(\mathbf{k}) &= 2(t_\parallel \cos k_z + t_1 \cos k_x + t_2 \cos k_y) \sigma_0 + \Delta \sigma_3 \\ &\quad - 2t_\perp (\sin k_x \sigma_1 + \sin k_y \sigma_2). \end{aligned} \quad (11)$$

The Fermi surface at  $E = 0$  is shown in Fig. 1(c).

The above models respect only one of the four (particle-hole or chiral) symmetries, Eqs. (2), (3), (4), or (5). If there were time reversal symmetry  $\mathbb{T}$ ,  $\mathbb{T}\mathbb{H}^T\mathbb{T}^{-1} = \mathbb{H}$ , combining  $\mathbb{T}$  and the particle-hole or chiral symmetry should give rise to another chiral or particle-hole symmetry. Having only one particle-hole or chiral symmetry, therefore, means TRS is broken. In Appendix A, we explicitly demonstrate the broken-time-reversal symmetries in the these three models, by showing the non-zero Hall conductivity calculated from the Berry phase of Bloch bands.

### III. ORTHOGONAL MODELS WITH PARTICLE-HOLE OR CHIRAL SYMMETRIES

In this chapter, we introduce two-orbital tight-binding models that belong to two orthogonal classes CI and BDI with chiral and particle-hole symmetries. The two models are real-valued and symmetric, hence chiral and particle-hole symmetries are equivalent. In the following two models, the random potential  $\epsilon_i$  takes the same uniform distribution as in Eq. (1). The class CI model is

given as follows,

$$\begin{aligned} H_{\text{CI}} &\equiv \sum_{\mathbf{i}, \mathbf{j}} \sum_{d, d'=a, b} |\mathbf{i}, d\rangle [\mathbb{H}_{\text{CI}}]_{(\mathbf{i}, d | \mathbf{j}, d')} \langle \mathbf{j}, d' | \\ &= \sum_{\mathbf{i}} (\epsilon_i + \Delta) (|\mathbf{i}, a\rangle \langle \mathbf{i}, b| + |\mathbf{i}, b\rangle \langle \mathbf{i}, a|) \\ &\quad + \sum_{\mathbf{i}} \left\{ \sum_{\mu=x, y} t_\perp (|\mathbf{i} + \mathbf{e}_\mu, a\rangle \langle \mathbf{i}, a| + |\mathbf{i} + \mathbf{e}_\mu, b\rangle \langle \mathbf{i}, b|) \right. \\ &\quad + t_\parallel (|\mathbf{i} + \mathbf{e}_z, a\rangle \langle \mathbf{i}, a| - |\mathbf{i} + \mathbf{e}_z, b\rangle \langle \mathbf{i}, b|) \\ &\quad \left. + t'_\parallel (|\mathbf{i} + \mathbf{e}_z, a\rangle \langle \mathbf{i}, b| + |\mathbf{i} + \mathbf{e}_z, b\rangle \langle \mathbf{i}, a|) + \text{H.c.} \right\}. \end{aligned} \quad (12)$$

It has only the following particle-hole (chiral) symmetry,

$$\mathbb{C}_3 \mathbb{H}_0^T \mathbb{C}_3^{-1} = -\mathbb{H}_0, \quad \mathbb{C}_3 = \delta_{\mathbf{i}, \mathbf{j}} (-1)^{i_x + i_y} [\sigma_2]_{d, d'}, \quad (13)$$

with  $\mathbb{C}_3^T = -\mathbb{C}_3$ . Note that there is no other particle-hole symmetries. Namely,  $\mathbb{C}_3$  must be diagonal with respect to the cubic-lattice site index, because of the on-site random terms. From the on-site term, it has to take a form of either  $\sigma_2$  or  $\sigma_3$  in the orbital space. From the nearest-neighbor hoppings within the  $x$ - $y$  plane, it comes with a U(1) phase of  $(-1)^{i_x + i_y} e^{i\theta(i_z)}$ . From the hopping along  $z$ , such  $\mathbb{C}_3$  is uniquely determined by  $(-1)^{i_x + i_y} \sigma_2$ , hence the model belongs to the symmetry class CI. In this paper, we take  $\Delta = t_\perp = t_\parallel = 1$ ,  $t'_\parallel = 2$ . The Fermi surface at  $E = 0$  is shown in Fig. 1(d).

The class BDI model is given by

$$\begin{aligned} H_{\text{BDI}} &\equiv \sum_{\mathbf{i}, \mathbf{j}} \sum_{d, d'=a, b} |\mathbf{i}, d\rangle [\mathbb{H}_{\text{BDI}}]_{(\mathbf{i}, d | \mathbf{j}, d')} \langle \mathbf{j}, d' | \\ &= \sum_{\mathbf{i}} (\epsilon_i + \Delta) (|\mathbf{i}, a\rangle \langle \mathbf{i}, a| - |\mathbf{i}, b\rangle \langle \mathbf{i}, b|) \\ &\quad + \sum_{\mathbf{i}} \left\{ \sum_{\mu=x, y} t_\perp (|\mathbf{i} + \mathbf{e}_\mu, a\rangle \langle \mathbf{i}, a| + |\mathbf{i} + \mathbf{e}_\mu, b\rangle \langle \mathbf{i}, b|) \right. \\ &\quad + t_\parallel (|\mathbf{i} + \mathbf{e}_z, a\rangle \langle \mathbf{i}, a| - |\mathbf{i} + \mathbf{e}_z, b\rangle \langle \mathbf{i}, b|) \\ &\quad \left. + t'_\parallel (|\mathbf{i} + \mathbf{e}_z, a\rangle \langle \mathbf{i}, b| - |\mathbf{i} + \mathbf{e}_z, b\rangle \langle \mathbf{i}, a|) + \text{H.c.} \right\}. \end{aligned} \quad (14)$$

It has only the following chiral (particle-hole) symmetry;

$$\mathbb{P}_3 \mathbb{H}_{\text{BDI}} \mathbb{P}_3^{-1} = -\mathbb{H}_{\text{BDI}}, \quad \mathbb{P}_3 = \delta_{\mathbf{i}, \mathbf{j}} (-1)^{i_x + i_y} [\sigma_1]_{d, d'}. \quad (15)$$

with  $\mathbb{P}_3^T = \mathbb{P}_3$ . Namely, from the first two terms of Eq. (14),  $\mathbb{P}_3$  must take a form of either  $(-1)^{i_x + i_y} e^{i\theta(i_z)} \sigma_1$  or  $(-1)^{i_x + i_y} e^{i\theta(i_z)} \sigma_2$ . The last two terms uniquely determine  $\mathbb{P}_3$  to be  $(-1)^{i_x + i_y} \sigma_1$ ; the model belongs to the symmetry class BDI. Here we take  $\Delta = t_\perp = t'_\parallel = 1$ ,  $t_\parallel = 0.5$ . The Fermi surface at  $E = 0$  is shown in Fig. 1(e).

We emphasize that the BdG symmetry classes describe the localization of Bogoliubov quasiparticle wavefunctions in superconductors [18], where disordered single-particle Hamiltonian is given by a mixed basis in particle

and hole space. In the class C, D and CI models introduced above, the particle and hole degrees of freedom are undertaken by the two orbitals. Thereby, the concept of a finite area of Fermi surface applies to single-particle wavefunctions of these two-orbitals models. We expect the critical behaviors of the Anderson transition of the single-particle wavefunctions are the same as those of the superconducting quasiparticle wavefunctions.

#### IV. METHOD AND RESULT

The scaling theory is at the heart of studying quantum criticality of the Anderson localization. On approaching the critical point, various physical quantities diverge according to a power law with the universal critical exponent  $\nu$ . One of them is the correlation length  $\xi \sim |x - x_c|^{-\nu}$ , which in a localized phase, characterises a decay length of a density-density correlation function in disordered medium. Here  $x$  represents the coordinate in a certain parameter space of the system and  $x_c$  stands for the critical point. To determine the critical exponent, we calculate a quasi-one-dimensional (Q1D) localization length  $\lambda$  of a single-particle wavefunction amplitude, using transfer matrix method [11, 12]. To be specific, we consider the Q1D geometry of the 3D cubic lattice ( $L_x \times L_y \times L_z$ ) with a cross-section  $L_x = L_y = L \ll L_z$ . In such geometry, all the eigenstates of the disordered Hamiltonian are localized in  $z$  direction,  $|\psi| \sim \exp(-|z - z_0|/\lambda)$ , with the localization length  $\lambda$ . The scaling argument around the critical point suggests that the localization length normalized by the linear dimension of the cross-section,  $\Lambda \equiv \lambda/L$  or  $\Gamma = \Lambda^{-1}$ , must be scale-invariant (independent of  $L$ ) at the critical point (see Fig. 2). Namely, numerical data of  $\Lambda$  for different cross-sectional size  $L$  must fit in so-called the one-parameter scaling function near the transition point [11–13],

$$\Lambda(W, L) = f(L/\xi(W)) \quad (16)$$

where  $f(x)$  is a universal scaling function for the normalized localization length.  $\xi(W)$  is the correlation length that depends on disorder strength:  $\xi(W) \sim |W - W_c|^{-\nu}$ . In practical calculations, one often encounters deviations of the data sets from the single-parameter scaling form. The deviations are attributed to finite-size effects associated with irrelevant scaling variables around the critical point in the framework of a renormalization group (RG) theory of general critical phenomena. In the RG theory, generic continuous phase transition is characterized by a saddle-point fixed point of RG equations for a certain effective theory with multiple system parameters. When high-energy degrees of freedom are integrated out, low-energy system parameters run away from the fixed point only along one direction in the parameter space, while they flow into the fixed point along all the other directions. The unstable direction around the fixed point is

characterized by relevant scaling variable, while its complementary directions are characterized by a number of irrelevant scaling variables. Scaling dimension of the relevant scaling variable is positive and it defines the universal critical exponent,  $1/\nu$ . Scaling dimensions of the irrelevant scaling variables are all negative, where the irrelevant variable with the largest negative scaling dimension is the least irrelevant. Empirically, we attribute the deviation of the numerical data from the single-parameter scaling to the least irrelevant scaling variable [14, 60]. The scaling argument that includes the effect of the least irrelevant scaling variable modifies the single-parameter scaling function form into

$$\Lambda(W, L) = F(u_1(w)L^{1/\nu}, u_2(w)L^{-y}), \quad (17)$$

where  $w = (W - W_c)/W_c$ , and  $1/\nu > 0$  and  $-y < 0$  are scaling dimensions of the relevant scaling variable  $u_1$  and the least irrelevant scaling variable  $u_2$ , respectively. The omission of the irrelevant scaling variables with smaller negative scaling dimensions are justified a posteriori by large  $y$  obtained from the fitting (see TABLE II).

To obtain the exponents  $\nu$ ,  $y$  as well as the scaling function  $f(x) \equiv F(x^{1/\nu}, 0)$ , we expand the scaling function  $F$  as Taylor series of its arguments

$$\Lambda = \sum_{i=0}^{n_1} \sum_{j=0}^{n_2} a_{ij} (u_1 L^{1/\nu})^i (u_2 L^{-y})^j. \quad (18)$$

When the system is close to the critical point, the scaling variables can be also expanded in small  $w$

$$u_1 = \sum_{k=1}^{m_1} b_k w^k, \quad u_2 = \sum_{k=0}^{m_2} c_k w^k. \quad (19)$$

To fix the ambiguity of fitting, we at  $a_{1,0} = a_{0,1} = 1$  [14, 60]. Having the polynomial form of the scaling function  $F$  in  $w$ , we use the least-squares fitting procedure and minimize  $\chi^2$  defined as follows,

$$\chi^2 = \sum_{i=1}^{N_D} \frac{(\Lambda_i - F_i)^2}{\sigma_i^2}. \quad (20)$$

Here  $\Lambda_i$ ,  $\sigma_i$ ,  $F_i$  are the numerical mean value of  $\Lambda$ , numerical standard error of  $\Lambda$ , and a fitting value of  $\Lambda$  from the polynomial fitting function. They are given at every data point specified by  $L$  and  $W$  with the data point index  $i = 1, \dots, N_D$ . The fitting results give estimate of  $\nu$ ,  $y$ ,  $W_c$ ,  $\Lambda_c$  and expansion coefficients  $\{a_{ij}\}$ ,  $\{b_k\}$ ,  $\{c_k\}$ . We choose  $n_1 = 3$ ,  $n_2 = 1$  and perform the polynomial fitting for different values of  $m_1$  and  $m_2$ . Results are shown in TABLE II. They are stable against changes of the expansion order  $m_1$ ,  $m_2$ , as well as the range of system sizes. The goodness of fit (GOF) is a probability that the  $N_D$  data points sampled from the fitting function would give a  $\chi^2$  larger than the minimized value  $\chi_{\min}^2$  of the fitting [61]. We use  $\Gamma$  as data inputs for the

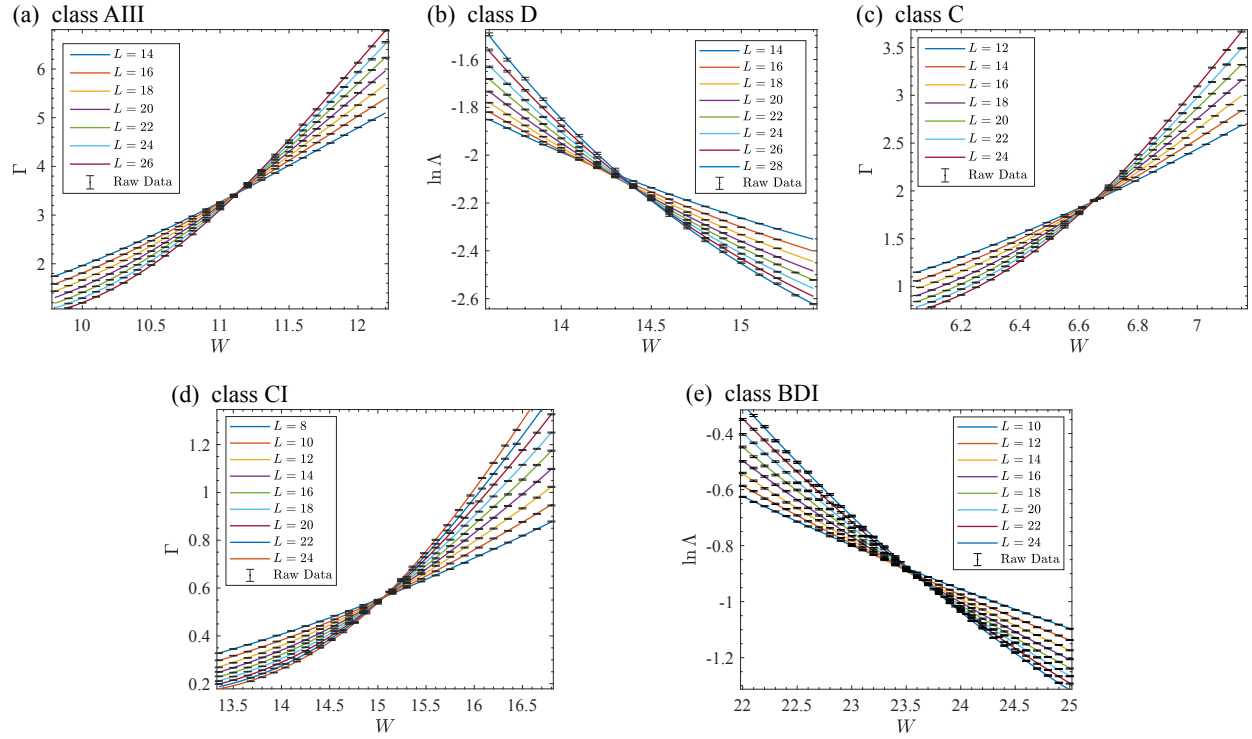


FIG. 2. Plots of normalized localization length (or its inverse or its logarithm) of the five models near the critical point of the Anderson transition for different system size in the transverse direction (see text).  $\Lambda$  is the dimensionless localization length and  $\Gamma = \Lambda^{-1}$ . Black dots are numerical data points with error bar and colored curves are the fitting results with the largest GOF in TABLE II. The quasi-one-dimensional samples are typically of length  $L_z = 10^6 - 10^7$  to ensure a 0.2 % precision of each data point.

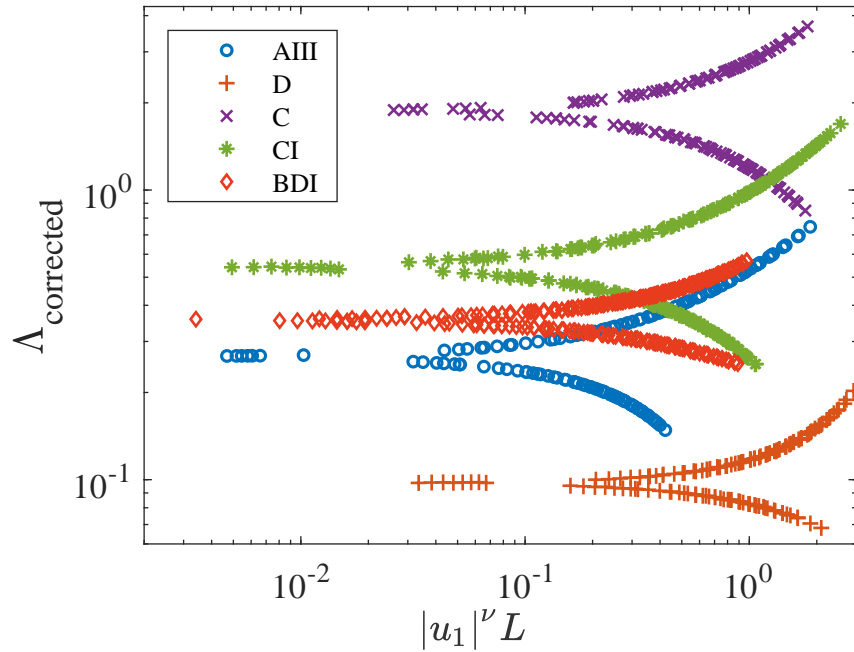


FIG. 3. The single-parameter scaling function of the normalized localized length for the five symmetry classes.  $\Lambda_{\text{corrected}}$  is the numerical data  $\Lambda$  subtracted by all terms of irrelevant scaling variable in Eq. (18). The upper branch is for the delocalized phase and the lower branch is for the insulator phase. We note that  $\Lambda_c$  depends on the anisotropy of the model.

evaluations in the class AIII, C and CI models, and in A for the class D and BDI models, in order to get better fitting qualities. The resulting critical exponents of the five symmetry classes are

$$\begin{aligned}
 \nu_{\text{AIII}} &= 1.06 \pm 0.02, \\
 \nu_{\text{D}} &= 0.87 \pm 0.03, \\
 \nu_{\text{C}} &= 0.996 \pm 0.012, \\
 \nu_{\text{CI}} &= 1.17 \pm 0.02, \\
 \nu_{\text{BDI}} &= 1.12 \pm 0.06.
 \end{aligned}
 \tag{21}$$

The numbers after  $\pm$  sign are the standard deviation determined from 1000 fittings of synthetic data sets.

The values of the evaluated critical exponents in the three non-standard symmetry classes with broken time-reversal symmetry are distinct from each other and also from previously evaluated critical exponents in other symmetry classes. The symmetry class C in 3D has been studied by network model of both quantum systems [62] and the classical counterpart [49]. The evaluated critical exponent in Ref. [49] is  $\nu = 0.9985 \pm 0.0015$ , which is in good agreement with our result. The symmetry class CI in 3D has also been studied with a lattice model [48] as  $\nu = 1.16 \pm 0.02$ , also in good agreement with our result. These consistencies demonstrate that the universality class of the Anderson transitions are free from details of the models, and it is determined only by the symmetry of the random matrices and the spatial dimension.

In Fig. 3, we show the scaling functions of these five non-standard symmetry classes. We define  $\Lambda_{\text{corrected}}$  from raw numerical data subtracted by the contributions of the irrelevant scaling variable in the fitting function  $F$ .  $\Lambda_{\text{corrected}}$  should obey the single-parameter scaling form in Eq. (16) around the critical point, with the scaling argument  $L/\xi \sim L|u_1|^\nu$ . When plotted as a function of  $L|u_1|^\nu$ ,  $\Lambda_{\text{corrected}}$  all collapse onto two branches of the scaling functions, where the upper (lower) branch corresponds to the metallic (localized) phase regime.

## V. SUMMARY AND DISCUSSION

In conclusion, we have clarified the universal critical exponents and scaling functions associated with the Q1D localization length of the 3D conventional localization-delocalization transition in three non-standard unitary symmetry classes (the chiral unitary classes AIII, the BdG class D and C), and in two non-standard orthogonal classes (the chiral orthogonal class BDI, the BdG class CI).

We introduced two-orbital tight-binding models on the cubic lattice that belong to these symmetry classes. In these models, the particle-hole degrees of freedom in usual BdG Hamiltonians for superconductors [18] and the sublattice degrees of freedom in usual chiral symmetry [9, 10, 63–65] are overtaken by an artificial orbital degrees of freedom. One of the advantages of these tight-binding models is that all of them have finite area

of Fermi surfaces in the clean limit. The presence of the finite Fermi surfaces in the clean limit guarantees the presence of 3D Anderson transitions at finite disorder strength. Using comprehensive numerical analyses, we (re)determine the critical exponents of the Anderson transition in these five non-standard symmetry classes. The exponents of the 3D class AIII and D are evaluated in this paper for the first time. The exponents of class C and CI are consistent with value in previous literature.

On the contrary, our exponent of the class BDI model is significantly different from a previous evaluation in the nodal Dirac semimetal (NDS) model [48]. The disordered NDS model has two topologically different types of delocalization-localization transitions in its phase diagram. One is a ‘topological’ phase transition line between diffusive metal (DM) phase and topological insulator (TI) phase with 1D topological winding number in the BDI class. The other is a ‘conventional’ phase transition line between the DM phase and ordinary (topologically trivial) band insulator or Anderson localized phase. The previous evaluation of the critical exponents at these two types of the phase transition lines are consistent with each other. On the one hand, the zero-energy density of state (DOS) suggests that the dynamical exponent at these two transitions could be different; the zero-energy DOS takes a finite constant value in the former ‘topological’ phase transition line, while the DOS shows a weak singularity at the zero energy around the ‘conventional’ phase transition line [48]. The singularity of the zero-energy DOS indicates a possible deviation of the dynamical exponent from the spatial dimension. It is an interesting open issue to study how the zero-energy DOS behaves at the Anderson transition point in the present BDI model. Such information could provide comprehensive understanding on the 3D Anderson transition in the BDI class.

Recently, the critical exponents and scaling functions in the non-standard symmetry classes acquire a lot of research interests from a view point of conventional and unconventional delocalization-localization transitions in non-Hermitian disordered systems. A previous dimensional regularization study of the non-linear sigma models in  $d = 2 + \epsilon$  shows that the  $\beta$  function in the three chiral symmetry classes is identical to zero [9, 10, 66]. The vanishing  $\beta$  function implies an unusual nature of delocalization-localization transition in these chiral symmetry classes [67]. Our evaluation of the universal critical properties provide solid information to these research community and will shed a new light in future experiments on quasiparticle heat transports in superconductors as well as the localization phenomena in random dissipative systems.

## ACKNOWLEDGMENTS

T. W. and R. S. thanks the fruitful discussion and correspondence with Xunlong Luo. T. O. was supported

TABLE II. Finite-size scaling analyses of the normalized localization length around the Anderson transition in the five non-standard symmetry classes. The scaling function of the normalized localization length is expanded in power of  $w \equiv (W - W_c)/W_c$  (see text). The expansion orders  $n_1 = 3$ ,  $n_2 = 1$  are fixed, while  $m_1, m_2$  are variables. The values inside the square brackets are 95% confidence intervals from 1000 Monte Carlo simulations. Only fitting samples with good of fit (GOF) greater than 0.1 are shown. We note that our model is anisotropic, and  $\Lambda_c$  depends on the anisotropy.

(a) 3D class AIII

$m_1$	$m_2$	$L$	GOF	$W_c$	$\nu$	$y$	$\Lambda_c$
2	0	12-26	0.308	11.247[11.226, 11.272]	1.059[1.022, 1.100]	0.814[0.585, 1.042]	0.248[0.234, 0.258]
2	0	14-26	0.475	11.223[11.201, 11.252]	1.071[1.033, 1.117]	1.326[0.975, 1.695]	0.262[0.251, 0.269]
3	0	12-26	0.290	11.255[11.234, 11.278]	1.069[1.030, 1.110]	0.726[0.527, 0.934]	0.244[0.228, 0.254]
3	0	14-26	0.479	11.213[11.193, 11.238]	1.055[1.013, 1.097]	1.572[1.144, 2.010]	0.266[0.257, 0.272]

(b) 3D class D

$m_1$	$m_2$	$L$	GOF	$W_c$	$\nu$	$y$	$\Lambda_c$
2	0	14-26	0.155	14.55[14.51, 14.61]	0.862[0.800, 0.903]	1.589[1.108, 2.069]	0.105[0.097, 0.109]
2	0	14-28	0.173	14.61[14.57, 14.67]	0.870[0.793, 0.928]	1.126[0.811, 1.444]	0.097[0.092, 0.103]
3	0	12-26	0.147	14.55[14.50, 14.61]	0.869[0.804, 0.915]	1.624[1.156, 2.113]	0.105[0.098, 0.109]
3	0	14-28	0.169	14.60[14.55, 14.66]	0.904[0.827, 0.967]	1.239[0.889, 1.587]	0.099[0.091, 0.104]

(c) 3D class C

$m_1$	$m_2$	$L$	GOF	$W_c$	$\nu$	$y$	$\Lambda_c$
3	1	12-24	0.313	6.641[6.637, 6.644]	0.9957[0.9711, 1.0184]	1.88[1.64, 2.38]	0.535[0.531, 0.538]
4	0	12-24	0.287	6.642[6.639, 6.645]	0.9972[0.9800, 1.0111]	2.86[2.43, 3.34]	0.533[0.531, 0.536]
4	1	12-24	0.295	6.641[6.639, 6.646]	0.9967[0.9738, 1.0207]	2.00[1.46, 2.57]	0.534[0.531, 0.538]

(d) 3D class CI

$m_1$	$m_2$	$L$	GOF	$W_c$	$\nu$	$y$	$\Lambda_c$
2	1	8-24	0.256	15.030[15.018, 15.043]	1.149[1.119, 1.177]	1.25[1.14, 1.62]	1.823[1.805, 1.840]
2	1	10-24	0.312	15.028[15.009, 15.048]	1.155[1.096, 1.187]	1.35[1.23, 1.77]	1.831[1.798, 1.851]
3	1	8-24	0.579	15.027[15.013, 15.041]	1.167[1.132, 1.198]	1.11[1.02, 1.49]	1.831[1.807, 1.850]
3	1	10-24	0.533	15.025[15.005, 15.047]	1.174[1.128, 1.215]	1.21[1.08, 1.76]	1.835[1.801, 1.864]

(e) 3D class BDI

$m_1$	$m_2$	$L$	GOF	$W_c$	$\nu$	$y$	$\Lambda_c$
2	1	10-24	0.522	23.859[23.803, 23.923]	1.104[0.940, 1.179]	1.02[0.77, 1.34]	0.356[0.338, 0.369]
2	1	12-26	0.311	23.895[23.857, 24.000]	1.116[0.915, 1.201]	1.04[0.845, 1.24]	0.351[0.337, 0.360]
3	1	10-24	0.548	23.859[23.756, 23.928]	1.119[0.973, 1.207]	1.01[0.76, 1.82]	0.356[0.338, 0.380]
3	1	12-26	0.325	23.896[23.856, 23.949]	1.115[0.903, 1.241]	1.04[0.85, 1.22]	0.351[0.337, 0.360]

by JSPS KAKENHI Grants 19H00658. T. W. and R. S. was supported by the National Basic Research Programs of China (No. 2019YFA0308401) and by National Natural Science Foundation of China (No.11674011 and No. 12074008).

### Appendix A: Berry Curvature and Time-reversal Symmetry

$H$  is time-reversal invariant, when it commutes with the time reversal operator  $\Theta$ ,

$$[\Theta, H] = 0, \quad \Theta = \mathbb{T} \cdot K, \quad (\text{A1})$$

where  $K$  is the complex conjugation and  $\mathbb{T}$  a unitary operator. Since the tight-binding models studied in this pa-

per contain on-site random potentials, the unitary transformation  $\mathbb{T}$  must be diagonal with respect to the lattice sites. To prove the absence of such  $\mathbb{T}$  in the class AIII and C models, we calculate the Hall conductivity at  $E = 0$  in the clean limit.

Two-bands Hamiltonians in the momentum space are written in the following form,

$$H(\mathbf{k}) = E_0(\mathbf{k})\sigma_0 + E_1(\mathbf{k})\mathbf{n}(\mathbf{k}) \cdot \boldsymbol{\sigma}. \quad (\text{A2})$$

with a three-component unit vector  $\mathbf{n}(\mathbf{k})$  and the two by two Pauli matrices  $\boldsymbol{\sigma}$ . For the 2 by 2 Hamiltonian, the two energy bands and the Berry curvature for each band

are given by

$$\begin{aligned} E_{\pm}(\mathbf{k}) &= E_0(\mathbf{k}) \pm E_1(\mathbf{k}), \\ \Omega_{xy}^{\pm}(\mathbf{k}) &= \pm \left( \frac{\partial \mathbf{n}}{\partial k_x} \times \frac{\partial \mathbf{n}}{\partial k_y} \right) \cdot \mathbf{n}. \end{aligned} \quad (\text{A3})$$

In terms of this, the Berry curvature of the class AIII model is calculated from Eq. (7),

$$\Omega_{xy}^{\pm}(\mathbf{k}) = \pm \frac{4t_{\perp}^2}{E_1^3} (\Delta \cos k_x + 2t) \cos k_y, \quad (\text{A4})$$

with  $E_1(\mathbf{k}) \equiv [(\Delta + 2t \cos k_x)^2 + 4t_{\perp}^2 (\sin^2 k_x + \sin^2 k_y)]^{1/2}$ . The Berry curvature of the class D model is calculated from Eq. (9),

$$\Omega_{xy}^{\pm}(\mathbf{k}) = \pm \frac{4t_{\perp}^2}{E_1^3} [\Delta \cos k_x \cos k_y + 2t(\cos k_x + \cos k_y)], \quad (\text{A5})$$

with  $E_1(\mathbf{k}) \equiv [(\Delta + 2t \cos k_x + 2t \cos k_y)^2 + 4t_{\perp}^2 (\sin^2 k_x + \sin^2 k_y)]^{1/2}$ . Likewise, the Berry curvature of the class C model is calculated from Eq. (11),

$$\Omega_{xy}^{\pm}(\mathbf{k}) = \pm \frac{4t_{\perp}^2}{E_1^3} \Delta \cos k_x \cos k_y, \quad (\text{A6})$$

with  $E_1(\mathbf{k}) \equiv [\Delta^2 + 4t_{\perp}^2 (\sin^2 k_x + \sin^2 k_y)]^{1/2}$ .

An integral of the Berry curvature over the occupied bands ( $E_{\pm} < 0$ ) is nothing but the Hall conductivity at  $E = 0$  at certain  $k_z$  [68],

$$\sigma_{xy}(k_z) \equiv \int_{E_+ < 0} d^2k \Omega_{xy}^+(\mathbf{k}) + \int_{E_- < 0} d^2k \Omega_{xy}^-(\mathbf{k}). \quad (\text{A7})$$

Throughout this paper we take lattice constant to be one, and the first Brillouin zone is  $k_{x,y,z} \in [-\pi, \pi]$ . By integrating over  $k_z$ , one gets the total Hall conductivity  $\sigma_{xy} = \int_{-\pi}^{\pi} dk_z \sigma_{xy}(k_z)$ . A non-zero Hall conductivity indicates the broken time-reversal symmetry. With the chosen parameters for numerical simulations of the three model, we get  $\sigma_{xy}/8\pi^2 \approx 0.04$  for the class AIII model,  $\sigma_{xy}/8\pi^2 \approx 0.73$  for the class D model, and  $\sigma_{xy}/8\pi^2 \approx 0.58$  for the class C model.

- 
- [1] P. W. Anderson, Phys. Rev. **109**, 1492 (1958).  
[2] F. Evers and A. D. Mirlin, Rev. Mod. Phys. **80**, 1355 (2008).  
[3] E. Abrahams, ed., *50 Years of Anderson Localization* (World Scientific Publishing Company, 2010).  
[4] F. J. Wegner, Zeitschrift fr Physik B Condensed Matter and Quanta **25**, 327 (1976).  
[5] E. Abrahams, P. W. Anderson, D. C. Licciardello, and T. V. Ramakrishnan, Phys. Rev. Lett. **42**, 673 (1979).  
[6] K. B. Effetov, A. I. Larkin, and D. E. Khmel'nitsukii, Soviet Phys. JETP **52**, 568 (1980).  
[7] S. Hikami, Phys. Rev. B **24**, 2671 (1981).  
[8] S. Hikami, Physics Letters B **98**, 208 (1981).  
[9] R. Gade and F. Wegner, Nucl. Phys. B **360**, 213 (1991).  
[10] R. Gade, Nucl. Phys. B **398**, 499 (1993).  
[11] A. MacKinnon and B. Kramer, Phys. Rev. Lett. **47**, 1546 (1981).  
[12] A. Mackinnon and B. Kramer, Zeitschrift Fur Physik B-Condensed Matter **53**, 1 (1983).  
[13] J.-L. Pichard and G. Sarma, J. Phys. C: Solid State Phys. **C14**, L127 (1981).  
[14] K. Slevin and T. Ohtsuki, Phys. Rev. Lett. **82**, 382 (1999).  
[15] E. P. Wigner, Mathematical Proceedings of the Cambridge Philosophical Society **47**, 790–798 (1951).  
[16] F. J. Dyson, Journal of Mathematical Physics **3**, 140 (1962).  
[17] F. J. Dyson, Journal of Mathematical Physics **3**, 1199 (1962).  
[18] A. Altland and M. R. Zirnbauer, Physical Review B **55**, 1142 (1997).  
[19] D. M. Basko, I. L. Aleiner, and B. L. Altshuler, Annals of Physics **321**, 1126 (2006).  
[20] J. A. Kjäll, J. H. Bardarson, and F. Pollmann, Phys. Rev. Lett. **113**, 107204 (2014).  
[21] R. Nandkishore and D. A. Huse, Annual Review of Condensed Matter Physics **6**, 15 (2015).  
[22] J. Billy, V. Josse, Z. Zuo, A. Bernard, B. Hambrecht, P. Lugan, D. Clément, L. Sanchez-Palencia, P. Bouyer, and A. Aspect, Nature **453**, 891 (2008).  
[23] G. Modugno, Reports on Progress in Physics **73**, 102401 (2010).  
[24] L. Sanchez-Palencia, D. Clément, P. Lugan, P. Bouyer, and A. Aspect, New Journal of Physics **10** (2008), 10.1088/1367-2630/10/4/045019.  
[25] S. John, Phys. Rev. Lett. **58**, 2486 (1987).  
[26] D. S. Wiersma, P. Bartolini, A. Lagendijk, and R. Righini, Nature **390**, 671 (1997).  
[27] M. Segev, Y. Silberberg, and D. N. Christodoulides, Nature Photonics **7**, 197 (2013).  
[28] A. Mafi, Advances in Optics and Photonics **7**, 459 (2015).  
[29] S. E. Skipetrov and I. M. Sokolov, Phys. Rev. Lett. **114**, 053902 (2015).  
[30] S. E. Skipetrov, Phys. Rev. Lett. **121**, 093601 (2018).  
[31] T. R. Kirkpatrick, Phys. Rev. B **31**, 5746 (1985).  
[32] R. Weaver, Wave Motion **12**, 129 (1990).  
[33] H. Hu, A. Strybulevych, J. H. Page, S. E. Skipetrov, and B. A. van Tiggelen, Nature Physics **4**, 945 (2008).  
[34] K. Slevin and T. Ohtsuki, Journal of the Physical Society of Japan **85**, 104712 (2016).  
[35] K. Slevin and T. Ohtsuki, Journal of the Physical Society of Japan **87**, 094703 (2018), <https://doi.org/10.7566/JPSJ.87.094703>.  
[36] Y. Asada, K. Slevin, and T. Ohtsuki, J. Phys. Soc. Jpn. **74**, 238 (2005).  
[37] B. Roy, Y. Alavirad, and J. D. Sau, Phys. Rev. Lett.

- 118**, 227002 (2017).
- [38] P. Heinzner, A. Huckleberry, and M. R. Zirnbauer, *Communications in Mathematical Physics* **257**, 725 (2005).
- [39] K. Kawabata and S. Ryu, *Phys. Rev. Lett.* **126**, 166801 (2021).
- [40] B. Xu, T. Ohtsuki, and R. Shindou, *Phys. Rev. B* **94**, 220403 (2016).
- [41] A. F. Tzortzakakis, K. G. Makris, and E. N. Economou, *Phys. Rev. B* **101**, 014202 (2020).
- [42] C. Wang and X. R. Wang, *Phys. Rev. B* **101**, 165114 (2020).
- [43] Y. Huang and B. I. Shklovskii, *Phys. Rev. B* **101**, 014204 (2020).
- [44] Y. Huang and B. I. Shklovskii, *Phys. Rev. B* **102**, 064212 (2020).
- [45] X. Luo, T. Ohtsuki, and R. Shindou, *Phys. Rev. Lett.* **126**, 090402 (2021).
- [46] X. Luo, T. Ohtsuki, and R. Shindou, “Transfer matrix study of the anderson transition in non-hermitian systems,” (2021), arXiv:2103.05239 [quant-ph].
- [47] H. Cao, Y. G. Zhao, S. T. Ho, E. W. Seelig, Q. H. Wang, and R. P. H. Chang, *Phys. Rev. Lett.* **82**, 2278 (1999).
- [48] X. Luo, B. Xu, T. Ohtsuki, and R. Shindou, *Phys. Rev. B* **101**, 020202 (2020).
- [49] M. Ortuño, A. M. Somoza, and J. T. Chalker, *Phys. Rev. Lett.* **102**, 070603 (2009).
- [50] I. Mondragon-Shem, T. L. Hughes, J. Song, and E. Prodan, *Phys. Rev. Lett.* **113**, 046802 (2014).
- [51] J. Song and E. Prodan, *Phys. Rev. B* **89**, 224203 (2014).
- [52] L. Li, C. Yin, S. Chen, and M. A. N. Araújo, *Phys. Rev. B* **95**, 121107 (2017).
- [53] B. Sbierski, J. F. Karcher, and M. S. Foster, *Phys. Rev. X* **10**, 021025 (2020).
- [54] J. Claes and T. L. Hughes, *Phys. Rev. B* **101**, 224201 (2020).
- [55] G. M. Luke, Y. Fudamoto, K. M. Kojima, M. I. Larkin, J. Merrin, B. Nachumi, Y. J. Uemura, Y. Maeno, Z. Q. Mao, Y. Mori, H. Nakamura, and M. Sigrist, *Nature* **394**, 558 (1998).
- [56] J. Xia, Y. Maeno, P. T. Beyersdorf, M. M. Fejer, and A. Kapitulnik, *Phys. Rev. Lett.* **97**, 167002 (2006).
- [57] E. R. Schemm, W. J. Gannon, C. M. Wishne, W. P. Halperin, and A. Kapitulnik, *Science* **345**, 190 (2014).
- [58] S. Liu, T. Ohtsuki, and R. Shindou, *Phys. Rev. Lett.* **116**, 066401 (2016).
- [59] A. A. Burkov and L. Balents, *Phys. Rev. Lett.* **107**, 127205 (2011).
- [60] K. Slevin and T. Ohtsuki, *New J. Phys.* **16**, 015012 (2014).
- [61] P. Bevington and D. Robinson, *Data Reduction and Error Analysis for the Physical Sciences* (McGraw-Hill Education, 2003).
- [62] V. Kagalovsky, B. Horovitz, and Y. Avishai, *Phys. Rev. Lett.* **93**, 246802 (2004).
- [63] J. J. M. Verbaarschot and I. Zahed, *Phys. Rev. Lett.* **70**, 3852 (1993).
- [64] J. J. M. Verbaarschot and I. Zahed, *Phys. Rev. Lett.* **73**, 2288 (1994).
- [65] K. Slevin and T. Nagao, *Phys. Rev. Lett.* **70**, 635 (1993).
- [66] F. Wegner, *Nuclear Physics B* **316**, 663 (1989).
- [67] E. J. König, P. M. Ostrovsky, I. V. Protopopov, and A. D. Mirlin, *Phys. Rev. B* **85**, 195130 (2012).
- [68] D. J. Thouless, M. Kohmoto, M. P. Nightingale, and M. den Nijs, *Phys. Rev. Lett.* **49**, 405 (1982).